Geophys. J. Int. (2002) **151,** 543–565

Ocean-bottom seismograph tomographic experiments—a consideration of acquisition geometries vs. resources

Christine Peirce and Anthony J. Day*

Department of Geological Sciences, University of Durham, Science Laboratories, South Road, Durham, DH1 3LE, *UK.*
E-mail: Christine.Peirce@durham.ac.uk

Accepted 2002 June 7. Received 2002 May 13; in original form 2001 May 9

SUMMARY

Over the last 20–30 yr numerous seismic images of the Earth's crust have revealed details of its gross structure, including intra-crustal layering, the geometry of that layering and its composition. As more and higher quality studies are undertaken it is becoming apparent that identified structures have a greater degree of 3-D variability than first anticipated. Thus, the methodology of crustal imaging by seismic means has also developed into the third dimension with a tomographic approach now being widely adopted, particularly so in the marine environment. Such surveys not only focus on mapping the finer scale 3-D structural variability, they also aim to achieve sufficient density of azimuthal coverage and resolution to address preferential orientation patterns of features such as porosity, fracturing and faulting.

Recent developments in technology, and consequently cheaper construction and deployment costs of instruments, have resulted in an expansion in the number of instruments available in ocean-bottom seismometer pools. Consequently, individual experiments are being designed to accommodate the maximum number of instruments available and this, coupled with dense grids of shot profiles, significantly impacts on survey cost. In this paper we consider a variety of approaches to achieving the best resolution of detail for minimal associated cost of acquisition, and for instrument pools of various sizes. A number of different geometries are compared, including example grid designs in current use. Comparison of resolution tests and relative costings for a range of acquisition geometries suggest that, if instrument numbers and/or funds are limited, the most cost effective ways of achieving the desired target resolution may be by (1) shooting additional shot profiles at the expense of deploying more instruments and (2) multiple, overlapping deployments of a small geometry, tailored in shape to the target structure and depth.

Key words: acquisition geometry, ocean-bottom seismology, seismic tomography.

1 INTRODUCTION

As our knowledge of crustal structure improves hand-in-hand with the ever-increasing number of geophysical, geological and geochemical surveys, it is becoming clear that lateral and vertical intra-crustal structure and properties are far more variable than once thought. To address this variability, wide-angle seismic experimental geometries have been adapted from the more traditional 2-D style, where data are collected solely along a series of linear profiles, to 3-D where data are acquired in a more areal fashion. The latter approach has been made possible by technical advances and a greater degree of versatility and general increase in numbers of instruments in accessible equipment pools.

In the case of crustal seismic tomography, whether on land or at sea, the 3-D approach to acquisition has resulted in an associated increase in experimental costs. In the marine case in particular, using ocean-bottom seismographs (OBS), the 3-D approach has resulted in the desire to access a large number of instruments (50–100+) and, consequently, a greater number of ship days for deployment and shot firing along the associated network of profiles. Although currently there are a few instrument pools that comprise in excess of 100 OBS, many national and research group pools average around 20–30 instruments and are likely to remain so for some time to come. Thus, the desire for large numbers of instruments necessitates internation, or inter-group collaborations or hire arrangements.

The purpose of this paper is to consider whether similar, or at least acceptable, resolution of an example target structure may be achieved with instrument numbers typical of research group or national pools to that obtained by a dense grid packed with 50 or more instruments.

*Present address: PGS Research, PGS Court, Halfway Green, Walton on Thames, Surrey, KT12 1RS.

2 EXAMPLE STRUCTURE AND BASIS OF ANALYSIS

For this consideration of acquisition geometries, we require a laterally and vertically variable example structure, which contains a variety of features at a range of length scales and target depths. One such example is a mid-ocean ridge, whose topography also provides a means by which the effect of seabed geometry on ray coverage and resolution may also be investigated. Here we will use the Central Valu Fa Ridge (CVFR), an intermediate-spreading ridge in the Lau Basin, as our example.

In 1995, a cruise aboard the *R/V Maurice Ewing* (EW9512—Peirce *et al.* 1996) adopted a primarily two profile 2-D approach to acquire a wide-angle seismic data set across this ridge using OBS (Fig. 1). However, a number of additional axis-parallel and perpendicular lines were also shot with the intention of providing a degree of 3-D coverage of the ridge axis, particularly so over a target region encompassing the oceanic crustal layer 2/3 boundary

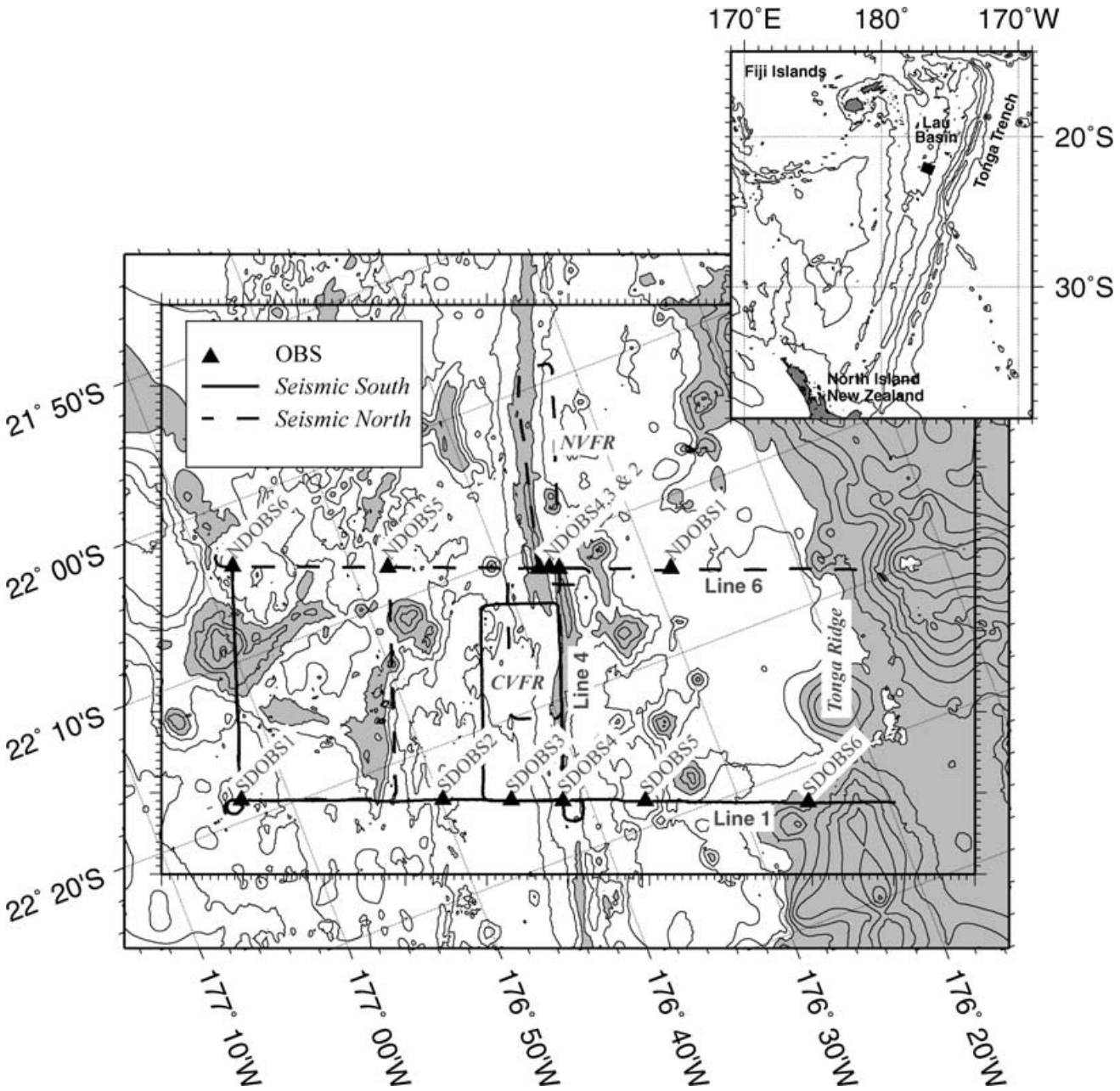

Figure 1. Experimental configuration of the Central Valu Fa Ridge seismic study (after Peirce *et al.* 1996; Turner *et al.* 1999). Shot profiles are denoted by solid (*Seismic South*) and dashed (*Seismic North*) lines, and the main 2-D seismic profiles are annotated. Bathymetric contours at 250 m intervals have also been plotted, and seabed depths shallower than 2000 m have been shaded to show the locations of the Central (CVFR) and Northern (NVFR) Valu Fa Ridges and Tonga arc. Ocean-bottom seismograph deployment positions are shown by triangles. The boxed region, graduated at 1 km intervals, shows the initial model dimensions in the horizontal plane (*cf*. Fig. 2). The inset shows the geographic location of the Valu Fa Ridge in the Lau Basin, with the actual survey area marked by the black box.

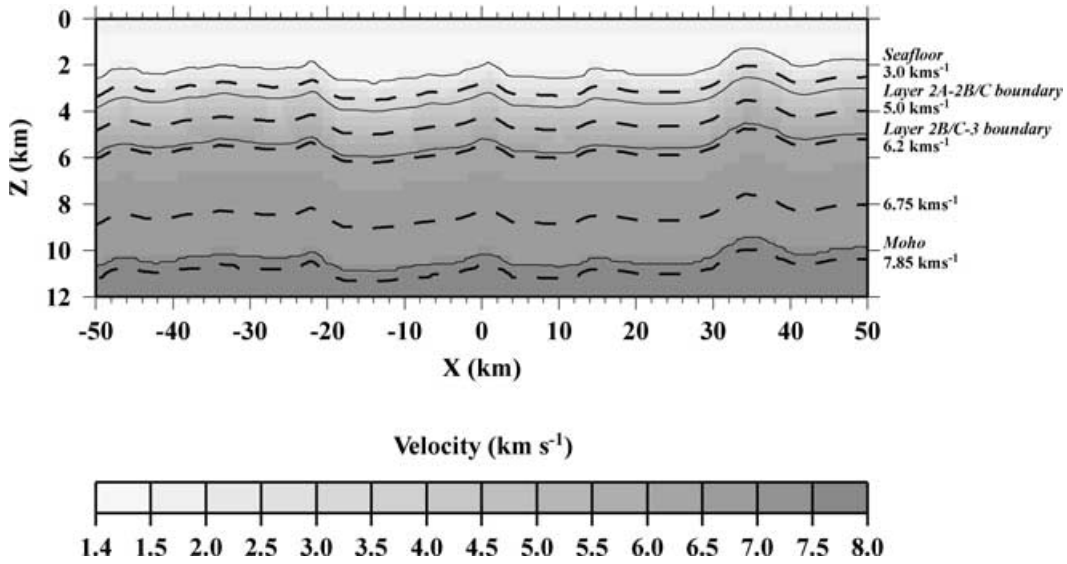

Figure 2. Central Valu Fa Ridge across-axis initial model for geometry analysis inversion. Cross-section at $y = 0$ km (*cf.* Fig. 3) showing the principal layer boundaries (solid lines) and the positions of the 3.0, 5.0, 6.2, 6.75 and 7.85 km s^{-1} constant velocity planes (dashed lines). See text for details. Vertical exaggeration—×3. Axes are annotated in model dimensions: *z*–depth; *x*–across-model offset; *y*–along-model offset.

and the uppermost part of layer 3—the target depth. Thus, although this experiment was primarily traditional 2-D in nature it was also 3-D in the most minimal sense. Analysis of the acquired wide-angle seismic data, following the more traditional 2-D forward modelling approach (Lines 1 and 6 of Fig. 1, Turner 1998; Turner *et al.* 1999), suggested significant lateral and vertical variation in structure along-axis between the two across-axis 2-D profiles. This observation is common in 2-D surveys where inferences must then be made between these isolated 'sample' points. Day (2001) and Day *et al.* (2001) attempted to address this problem by adopting a 3-D tomographic approach to the analysis of the same data set, primarily with the view of investigating the variation in structure along-axis between the two 2-D profiles. As such, the combined work of Turner (1998) and Day (2001) at the Central Valu Fa Ridge (CVFR) provides an indication of the limitations of the 2-D approach to data acquisition and what is achievable with even the most minimalistic 3-D approach. Turner (1998) (Fig. 2) and Day (2001) results, together with a dense regional bathymetric data set (Zellmer *et al.* 1998), thus provide a detailed crustal model upon which to base the ray coverage and resolution analysis of a variety of 3-D acquisition geometries.

When undertaking a 3-D tomographic inversion by whatever method (e.g. Toomey *et al.* 1994; Zelt & Barton 1998) it is important that the starting, or initial, model for that inversion represents a reasonable estimate of the structure being investigated. This model may, primarily, be obtained by 1-D or 2-D analysis and modelling of data acquired along individual profiles within the survey area. Preferably profiles should be chosen which traverse typical or representative parts of the structure being modelled, or the background crust upon which the structure is superimposed. In this way much of the vertical variation may be accommodated from the outset, with the inversion process primarily left to resolve lateral variation. From this point of view, when designing an acquisition geometry it is, therefore, important to include a subset of instruments and shot profiles that provide 2-D coverage at least perpendicular to the strike of the (linear) structure being studied and preferably along the strike of the structure as well. Therefore, in addition only geometries comprising linear profiles will be considered here because it is common practice to collect other geophysical data sets contemporaneously in order to better constrain the starting velocity model (particularly at shallow crustal levels) or resolve ambiguities in the resulting velocity anomaly field. For example, in sedimented areas multichannel seismic data may be used to resolve sediment thickness and layering, or in the case of oceanic crustal surveys sonobuoys may be used to constrain the velocity structure in the shallowest levels and along shot profiles that do not traverse instrument positions. In addition, gravity data modelling may be used to provide an estimate of crustal thickness for initial model construction. Such data are normally acquired, analyzed and modelled primarily along linear profiles.

3 COMPARISON OF ACQUISITION GEOMETRIES

To compare the effectiveness of the more commonly adopted approaches to 3-D acquisition, resolution tests have been performed for a number of typical acquisition geometries using the method described by Zelt (1998). A model of dimensions 100 × 70 × 12 km, with *x*- and *y*-axes perpendicular and parallel to the CVFR respectively, was created extending sufficiently far off-axis to allow longer offset shot-receiver pairs, which sample the deeper crustal levels and into the uppermost mantle, to be included in the synthetic inversions in order to investigate the resolution at these depths (*cf.* Figs 1 and 2). Within this area the seabed was constructed from bathymetry data obtained from the regional compilation of Zellmer *et al.* (1998), which was also used for each proposed acquisition geometry to determine instrument deployment depths. The 1-D initial model of Day *et al.* (2001) was used to construct the crustal part of the initial model (Fig. 2). However, the model of Day *et al.* (2001) does not include a velocity discontinuity associated with the Moho, as its inclusion resulted in rays being predicted to travel through the mantle that were not observed in the CVFR data set. The lack of observed mantle arrivals results from the shot-receiver

offsets which Day *et al.* (2001) analyzed being less than the offset at which the triplication between crustal diving rays, mantle diving rays and Moho reflections occurs. Thus, as the initial model created for this analysis extends to sufficient offset to include lower crust and upper-mantle arrivals, a velocity discontinuity at the Moho has been included to allow resolution in the lowermost crust and uppermost mantle to be assessed in addition to that at shallower crustal levels. A shot spacing of 200 m (equivalent to the EW9512 experiment) was chosen for each of the profile lines and, to investigate 'best possible outcome' scenarios, 100 per cent data recovery was assumed for shots between 4 and 50 km offset from each receiver. An offset of 4 km is representative of the typical minimum shot-receiver offset at which crustal refracted arrivals are visible ahead of the direct water wave arrivals at the CVFR, i.e. the minimum offset at which crustal arrival travel times can be picked. The 50 km maximum shot-receiver offset was chosen, based on the real EW9512 data, to reflect the maximum offset at which arrivals are clearly detectable and reliably identifiable when using an airgun array as source. This is not to say that, in reality, arrivals of lower-signal-to-noise would not be observed beyond this offset, just that it would be safe to expect them to be observed to this offset as a bare minimum and that they would be associated with acceptable traveltime pick errors. Thus the resolution tests undertaken should reflect the resolution realistically achievable for each example geometry.

Synthetic first arrival traveltime data were obtained by ray tracing though the initial model and using the finite difference traveltime calculation method described by Vidale (1990) and Zelt & Barton (1998). For this calculation the initial model was perturbed in a checkerboard fashion as described by Zelt (1998). The eight checkerboard patterns comprise:

(1) the initial model with a ± 5 per cent velocity anomaly applied that is sinusoidally varying in both the x and y directions;

(2) the same model as (1) with the velocity anomaly polarity reversed;

(3, 4) the same as (1) and (2) except shifted in the x and y direction by a quarter of the wavelength of the sinusoidal anomaly;

(5–8) the same as (1)–(4) except with the anomaly pattern rotated through 45°.

Each checkerboard pattern was applied with cell sizes of 3, 5, 7, 10 and 15 km, where cell size is defined as half the wavelength of the sinusoidal anomaly. An uncertainty of 0.040 s, equivalent to the mean uncertainty of the real CVFR data (Day 2001), was associated with each resulting synthetic arrival and Gaussian noise added to the synthetic traveltime data with a standard deviation equal to this uncertainty. Although data uncertainty might be expected to increase with shot-receiver offset due to a general decrease in signal-to-noise ratio, no such systematic relationship was observed for the real EW9512 data (Day 2001). However, given that this relationship is considered normally to be the case, the assumption of a constant uncertainty implies that, for the examples shown, model resolution may be slightly overestimated at deep levels and similarly slightly underestimated at shallow levels. The synthetic traveltime data were then inverted using the method of Zelt & Barton (1998). A node spacing of 400 m was used for the forward grid for reasons of computational efficiency as this grid size is adequate for calculating travel times given the data uncertainty.

To investigate the lateral resolution of each geometry, the semblance between the synthetic and recovered velocity anomalies (as outlined above) for each of the checkerboard patterns was calculated using a 5 km diameter circular operator in the horizontal plane centred on each model node. A 5 km operator was chosen because, for this crustal structure, it is large enough to be insensitive to noise and small enough to reflect the similarity between the synthetic and recovered anomalies (Zelt 1998). A semblance threshold of 0.7 thus represents the areal and vertical dimensions of anomalies whose locations may be adequately resolved (Zelt 1998) and 0.9 those whose magnitudes may be determined (Day 2001; Day *et al.* 2001). To obtain the lateral resolution, the semblance values for each of the eight patterns were averaged for each of the five cell sizes, and an interpolation made at each node to find the minimum cell size for which the mean semblance exceeds each of the thresholds. These cell sizes thus represent the lateral velocity anomaly resolution both in terms of dimension and magnitude.

For real experiments, the acquisition geometry will be limited mainly by the number of available instruments and ship time (both of which have financial dependence), although the characteristics of the seafloor may determine the practicality of instrument deployment in specific locations. Therefore, example experimental geometries which employ different numbers of shots and instruments will be compared, and naturally each may be adapted according to the limitations of the available time and instrumentation, the nature of the target and its depth below surface and the nature of the seafloor.

Fig. 3(a)–(j) shows 10 example experimental geometries overlain on the smoothed CVFR bathymetry for structural reference. Geometry names are quoted in italics for clarity. *EW9512* (Fig. 3a) is identical to the EW9512 experimental geometry and is included to test the theoretical resolution of an experiment designed primarily with 2-D acquisition in mind but with limited 3-D coverage at a specific target depth. Six grid geometries are included for comparison where instruments are deployed at the intersection of parallel and perpendicular shot profiles that define each grid. Instrument numbers are chosen to reflect those available to research groups and national pools. The *Small grid*, *Small grid with diagonals* and *Small dense grid* geometries (Figs 3b–d) use nine instruments, a typical number available to a small research group, and increasing numbers of shot profiles. The *Large grid* and *Large sparse grid* geometries (Figs 3e and f) use twenty instruments, more typical of smaller national pools, and a closer grid spacing designed to provide denser ray coverage over roughly the same area. These two groups of geometry thus allow the effect of shot profile spacing to be considered. However, as the global total number of instruments available increases, larger numbers are now being routinely deployed with many thousands of shots fired along a lattice of grid lines. Although instrument pools of greater than 100 instruments do exist, these are still few in number and will most likely remain so for the foreseeable future and their full deployment costs are prohibitive for many funding agencies. However, the number of national, or group, pools comprising 20–30 instruments is slowly increasing as are the opportunities to collaborate, or to hire these services if funding allows. To reflect this capability the *Dense grid* (Fig. 3g) uses 56 instruments and a much smaller intra-profile spacing.

Possible alternatives to the grid approach are the *Star* and *Overlapping star* geometries (Figs 3h and i) which use single and multiple deployments of 11 instruments and ship tracks defining a five-pointed star. Finally, the *Combined star and grid* geometry (Fig. 3j) incorporates a modified version of the *Star* geometry with additional shot profiles and instruments arranged asymmetrically in an irregular grid. For this particular geometry additional shot profiles have been located specifically to image notable features of this mid-ocean ridge example, e.g. the overlapping spreading centre located at 0,-12

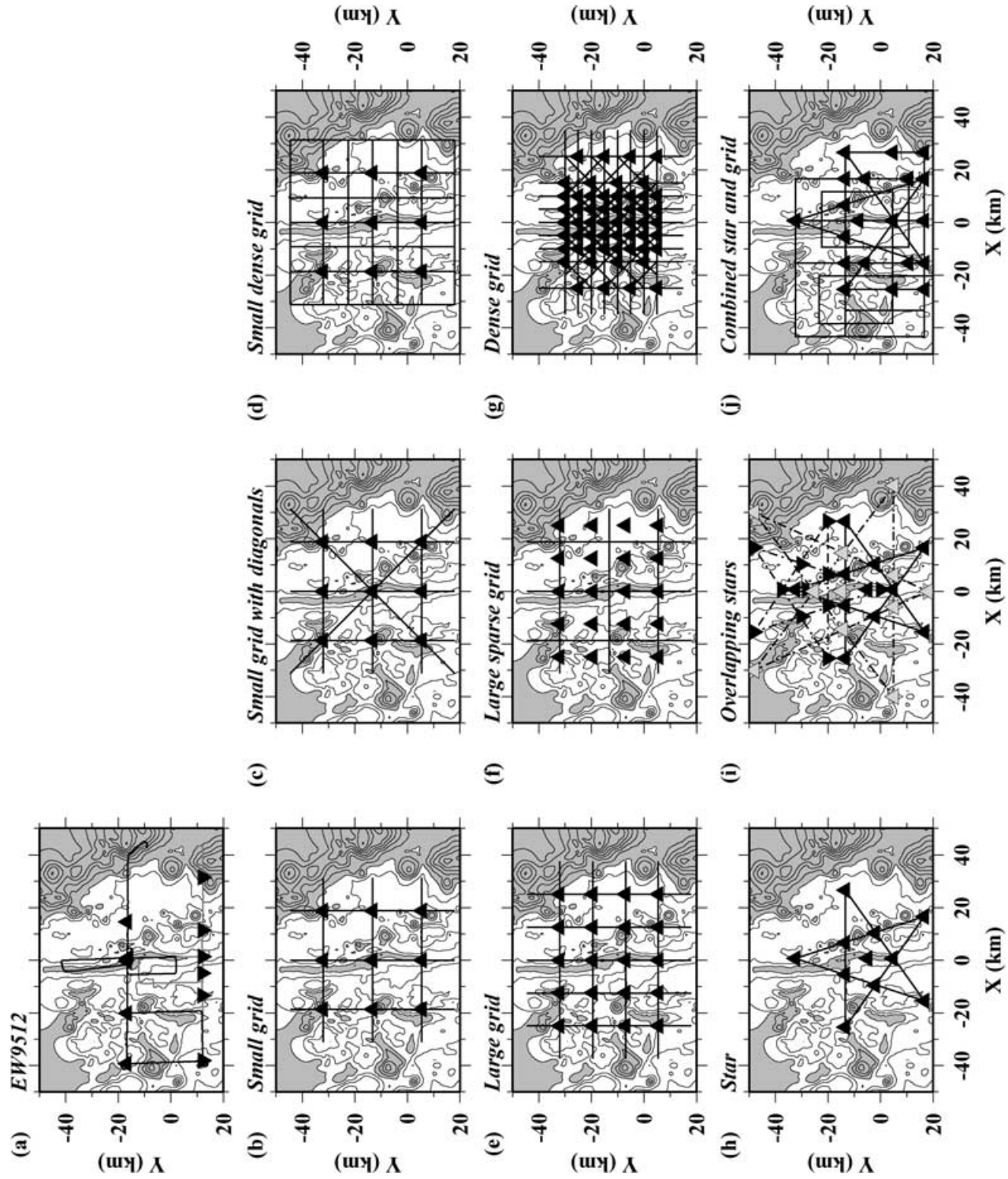

Figure 3. Trial acquisition geometries. Seabed bathymetry is included for structural reference with contours plotted at 250 m intervals. Triangles denote instrument positions, and lines shot profiles. See text for details. Inverted and grey triangles and grey or dashed lines respectively denote a multi-phase approach to acquisition.

model co-ordinates (Fig. 3j), these would thus be relocated to suit any particular target. The addition of extra profiles also provides a spiral capability for experiments where shot-receiver azimuth is also important. In addition, this geometry will be used to demonstrate that target-specific choice of profile and instrument location results in better coverage and more even, finer-scale lateral resolution. The numbers of instruments and shots required for each geometry are summarized in Table 2.

The resolution of each experimental geometry type will now be considered in turn. For all geometries, resolution is plotted for planes of constant velocity in the initial model at 3.0, 5.0, 6.2, 6.75 and 7.85 km s^{-1}. These planes are annotated on the cross-section through the initial model shown in Fig. 2 and correspond to the middle of layer 2A, middle of layer 2B, top of layer 3, middle of layer 3 and uppermost mantle respectively for this mid-ocean ridge example. When considering the resolution plots the focus of attention should be the region within the 'footprint' area defined by the outermost instrument locations, within which the target lies. The resolution outside these regions will have an associated inherent degree of ambiguity, in much the same way that an unreversed 2-D profile will be ambiguous without additional constraint. Thus, although the resolved structure at the lateral extremes will be less well constrained than elsewhere, it is certainly not unconstrained, provided that the initial model upon which the inversion is based is constrained as well as possible by additional, complementary data as already discussed.

3.1 Traditional 2-D

The *EW9512* geometry uses six instruments deployed twice, with a unique series of profiles shot for each deployment (dashed vs. solid lines in Fig. 1 or black vs. grey lines in Fig. 3a). As the EW9512 wide-angle seismic experiment was designed primarily with 2-D data acquisition in mind, ray coverage within the entire 3-D model volume is not optimum as Fig. 4 clearly shows. However, it is reasonable-to-good over the axial region of interest to this particular experiment, i.e. the structure at mid-crustal depths (layers 2B/C and 3– Figs 4b and c). Resolution, particularly in terms of velocity anomaly magnitude, in layer 2A is more variable and correlates with instrument locations. In addition, there is effectively a 'shadow' zone in coverage at lowermost crust and uppermost mantle depths correlating with the maximum shot-receiver offsets achievable with this geometry which relate, in turn, to the limited resources available for this acquisition necessitating that it be shot in two parts.

When assessing near surface resolution, Fig. 4(a) clearly shows that the nature and variation of the seabed bathymetry together with the inability to pick shallow crustal arrivals at near-instrument offsets due to the direct water wave arrival, are also important factors to consider. Day (2001) has shown that it is highly desirable that initial models contain a good representation of structure at depths shallower than the primary target. An accurate representation of shallow crustal structure may be achieved for acquisition geometries sparsely populated with instruments and shot profiles by acquiring additional data sets contemporaneously with shot firing as previously described. In addition, access to existing, or acquiring, swath bathymetry data within the acquisition 'footprint' allows prediction, assessment and minimization of errors in traveltime associated with imprecise knowledge of the seafloor ray entry point. This is particularly important in areas of rough seabed topography as is discussed at length by Sohn *et al.* (1997).

Comparison of Fig. 4 with the results of Day *et al.* (2001) shows that the theoretical resolution in the axial region is similar to that obtained for the real data. This observation implies that ray coverage geometry is the primary control on resolution rather than variations in data uncertainties resulting from, for example, inexact knowledge of shot and receiver positions, errors in traveltime picks in relation to signal-to-noise ratio etc., although they do of course contribute. Resolution away from the axial region is generally poorer, as would be expected with this geometry, and regions of good resolution tend to correlate with the 2-D profiles. Furthermore resolution in the lowermost crust (Fig. 4d) and uppermost mantle (Fig. 4e) is predicted to be quite poor. These findings suggest that, in instances such as this, there is little to be gained by extending the 3-D analysis of the EW9512 data set to greater than the primary target depth or further off-axis than the densest region of shot profiles between ~ -20 and 10 km ('east–west'). The latter also implies that sampling in the shot domain is more critical than in the receiver domain as receiver numbers will always be limited when compared to shot numbers.

This synthetic inversion alone highlights a number of issues that are pertinent to the design of 3-D acquisition geometries, and to the consideration of whether useful, or meaningful, results can be achieved when instrument and shooting resources are limited for whatever reason. Coupled with the work of Day *et al.* (2001), the results for this geometry show that meaningful 3-D crustal velocity models can be obtained if the initial model provides a realistic representation of, primarily, the vertical variation in structure. In this case, the initial model was created from the Turner *et al.* (1999) analysis of the EW9512 2-D profiles coupled with analysis of the results of early inversions which suggested, and provided constraint on, along-ridge variation—a forward-type approach to optimizing the nature of the initial model. In addition, along-ridge layer thickness and properties were derived from the Collier & Sinha (1992) and Day (1997) analysis and modelling of multichannel seismic and sonobuoy data acquired in the same location during RRS Charles Darwin CD34/88. Thus, when designing an acquisition geometry not only is it important to include simple 2-D profiles across the structure with which to develop the initial model and provide control on vertical variation and the geometry of structures at depth, it is equally important to include some means by which to determine a reliable estimate of shallow structure beneath shots and between instrument locations. This example shows that, by careful choice of shot profile location and the inclusion of complementary data, it is possible to achieve adequate coverage and resolution of a specific target structure with relatively few shots and receivers. A resolution of better than 5 km has been achieved for the structural target of interest (the Central Valu Fa Ridge axis) down through layers 2A, 2B/C and into layer 3– i.e. in the case of the CVFR, the top of the axial magma chamber and the melt migration path to the surface. Thus, if a target has a limited lateral extent relative to the acquisition 'footprint' and a specific, or limited, vertical extent then this type of approach would provide an adequate (though not ideal) and appropriate data set to invert.

3.2 Grid patterns

Grid geometries are now commonly employed for 3-D data acquisition as their simplicity allows interpretation in 2-D and 3-D as required and, as shot profiles usually traverse instrument locations, shallow crustal structure is generally also reasonably well constrained, provided that shot profiles and instruments are positioned at suitable intervals. Thus the areal extent and depth of the target to be imaged and the required resolution, generally determines the number of instruments and shot profiles required, although it is becoming increasingly common for dense grids of instruments to be deployed (and profiles shot) as technological advances result

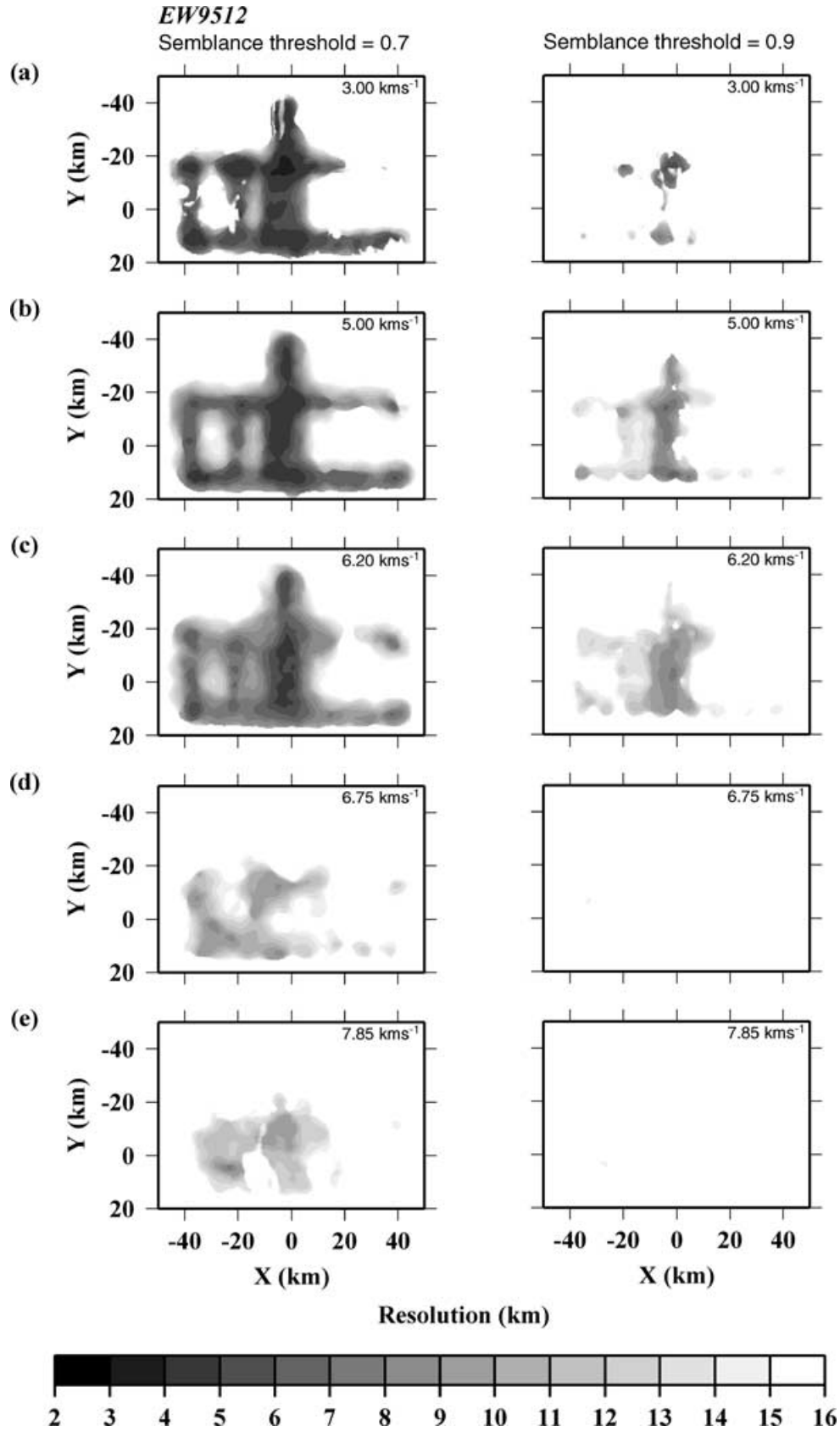

Figure 4. *EW9512* geometry. Lateral anomaly resolution determined with a semblance threshold of 0.7 (lateral extent—left) and 0.9 (magnitude—right) respectively for the constant velocity planes (a) 3.0, (b) 5.0, (c) 6.2, (d) 6.75 and (e) 7.85 km s^{-1} shown in Fig. 2. Black regions have a resolution better than 3 km and white worse than 15 km or are unsampled. Note that the ray coverage in the 3-D model volume is not smooth or continuous and that resolution at shallow levels is poor in places and instrument related, with a large degree of correlation with 2-D shot profiles.

Table 1. The six grid geometries.

Instrument numbers	Geometry	Details	
9—research group	*Small grid*	∼18.5 km instrument and profile spacing	Fig. 3(b)
	Small grid with diagonals	”	Fig. 3(c)
	Small dense grid	∼18.5 km instrument spacing plus ∼9.5 km profile spacing	Fig. 3(d)
20—small national pool	*Large grid*	∼12.5 km instrument and profile spacing	Fig. 3(e)
	Large sparse grid	∼12.5 km instrument spacing plus ∼18.5 km profile spacing	Fig. 3(f)
56—large national pool or consortium	*Dense grid*	∼2.5 km instrument spacing plus ∼5–10 km profile spacing	Fig. 3(g)

in cheaper instruments. However, increasing the number of instruments deployed and profile kilometres shot, increases not only the number of days of ship time required to undertake the acquisition (i.e. profile shooting, the deployment and recovery of instruments and the transit time between them) but also the total cost of consumables associated with instrument deployment.

Six grid geometries are considered here, which provide coverage over a similar ‘footprint’ area, and which employ different numbers of instruments and shot profiles such that a consideration of which approach provides the best resolution can be made in the context of cost effectiveness and value-for-money. Coupled with this, comparison of the resulting resolution plots will also provide a basis from which to consider whether acceptable resolution can, or cannot, be achieved with a relatively small number of instruments and/or shot profiles. The six grid geometries are outlined in Table 1.

3.2.1 Small grid geometries

The resolution of the *Small grid* geometry is shown in Fig. 5. Comparison with Fig. 4 shows a much improved velocity anomaly resolution over a greater area at lower crust and uppermost mantle depths (*cf.* Figs 4d and e and Figs 5d and e). Hence this geometry would be appropriate for investigating structure at these depths. However, at shallower levels (Figs 5a and b), although the resolution is better than for the *EW9512* geometry, the areas of highest resolution directly correspond with instrument and shot profile locations. This is a direct consequence of the distance between shot profiles being greater than the distance at which turning rays in the shallow crustal layers arrive. Hence there is a significant degree of 2-D bias, which implies that this geometry is only able to accurately constrain the structure of the uppermost crust in 2-D along the shot profiles. The uneven near-surface coverage may also make it difficult to distinguish real anomalies from inversion artefacts incorporated into the resulting model, which reflect this pattern of high and low data coverage and confidence levels. Of note also is that velocity anomaly magnitude (semblance threshold of 0.9) is only reasonably well resolved at the target mid-crustal levels (Fig. 5c right)—the 6.2 km s^{-1} plane (*cf.* Fig. 2b).

A possible solution to the problem of near-surface patchy coverage and resolution, without increasing instrument numbers, is to add additional shot profiles. To demonstrate this point the resolution of the *Small grid* geometry has been recalculated with two additional shot profiles included (*Small grid with diagonals*—Fig. 3c). These profiles run diagonally from each corner of the grid, with the primary aim of infilling the ‘holes’ in the ray coverage at shallow levels and short shot-receiver offset (Fig. 6). By comparison of Figs 5 and 6, the improvement in coverage and velocity anomaly resolution at shallow-mid structural levels is obvious, as is the improvement in confidence in magnitude recovery. Shallow resolution is still variable correlating with instrument position. However, more importantly, as shallow magnitude anomaly resolution improves the effect of seabed topography starts to become apparent.

At this point it is also instructive to consider the relative importances of sampling density in the shot and receiver domains. In the context of the *Small grid* geometries we will consider increasing the density of sampling in the shot domain by adding additional profiles at approximately half the original spacing. In this case the shallow regions beneath shot profiles which do not traverse instrument locations will not be directly constrained by the 2-D profile data recorded by instruments. Hence, in this case, it is assumed that alternative approaches to achieving shallow constraint as already described are adopted. The results of the resolution test for this *Small dense grid* geometry are shown in Fig. 7. The improvement in both velocity anomaly and velocity anomaly magnitude resolution is notable at all model levels as would be expected, with smooth and even coverage within the ‘footprint’ outlined by the instrument locations. The implications of this result will be discussed in the next section when considering increasing sampling in the receiver domain.

3.2.2 Large grid geometries

The *Large grid* geometry, shown in Fig. 3(e), includes twenty instruments (typical of a national pool) located at the intersection points of nine shot profiles. The spacing between shot profiles is similar to that of the *Small dense grid*. The resolution achieved with this geometry (Fig. 8) is significantly better than for either of the *EW9512* and *Small grid* geometries at all depths as would be expected, and is comparable to that for the *Small dense grid*. The smaller instrument and profile spacing of this geometry results in a denser ray coverage which, in turn, leads to a significant improvement in resolution at mid-lower crust and uppermost mantle depths throughout the region covered by the grid. However, by comparison with Fig. 7, this *Large grid* geometry still produces patchy coverage at shallow-mid crustal levels in both velocity anomaly and velocity anomaly magnitude, again resulting from the relative distance between shot profiles as described above.

The extent of coverage achieved by this geometry also nicely demonstrates how the seabed topography can effect the resulting resolution. The lateral variation in resolution on any given depth slice, particularly noticeable on the velocity anomaly magnitude plots, is mostly attributable to the effect of rough seafloor bathymetry on ray coverage since this geometry is otherwise totally regular and would, therefore, give rise to a regular resolution pattern if the seafloor were horizontal.

The *Large grid* geometry requires many more instruments and shots than any of the *Small grid*-type geometries. If instruments and ship time are limited, a trade-off between resolution at shallow and deeper levels will become inevitable, with the outcome

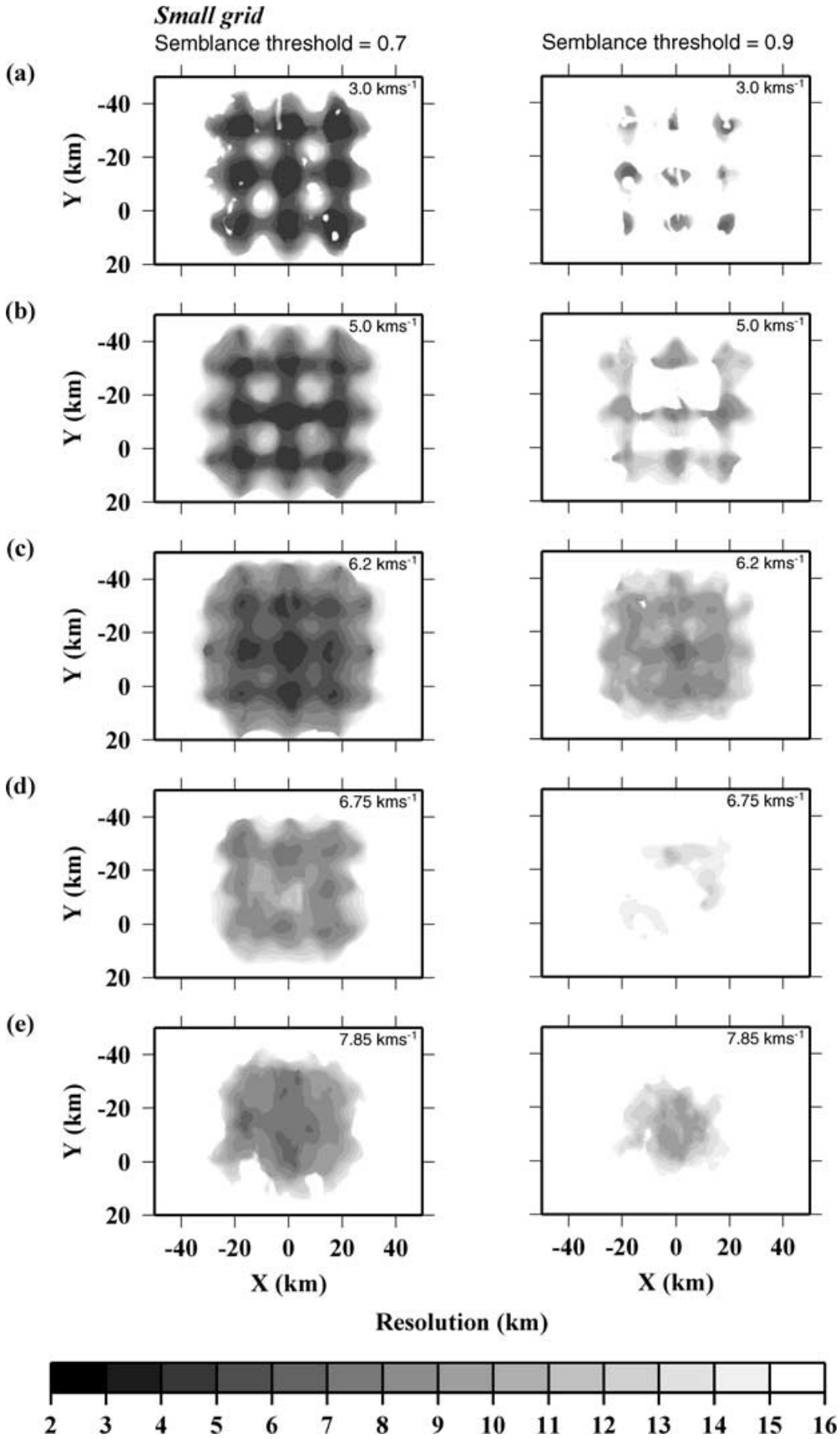

Figure 5. *Small grid* geometry. As for Fig. 4. Note the uneven, near-surface coverage and the 2-D bias related to instrument and shot profile locations. However, coverage and resolution at mid-lower crust and upper mantle levels is much better than for the *EW9512* geometry.

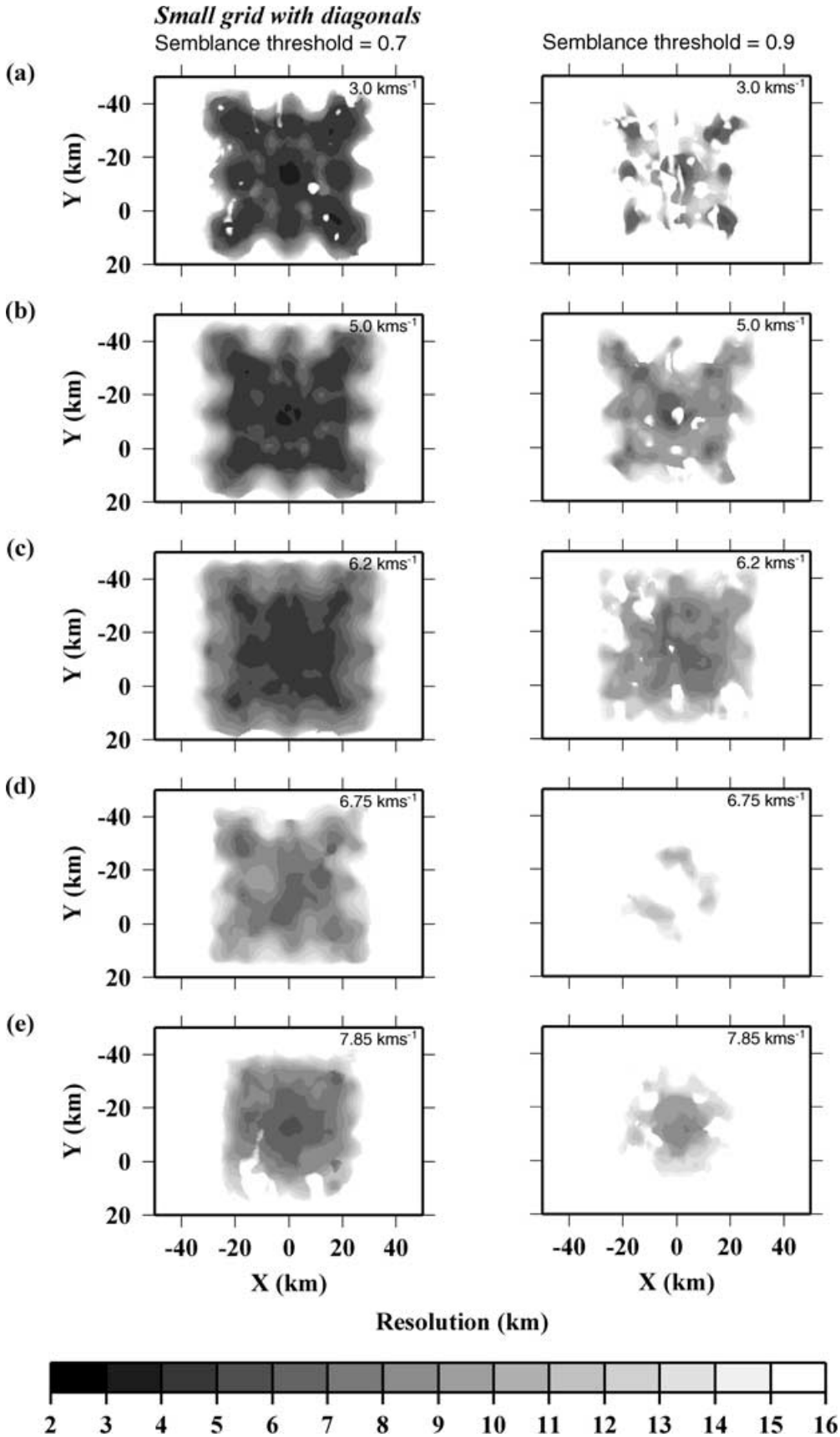

Figure 6. *Small grid with diagonals* geometry. As for Fig. 4. Note the improved resolution at all crustal levels compared with the *Small grid* geometry. Coverage and resolution are generally more even over a larger area and much of the 2-D instrument location bias has been removed.

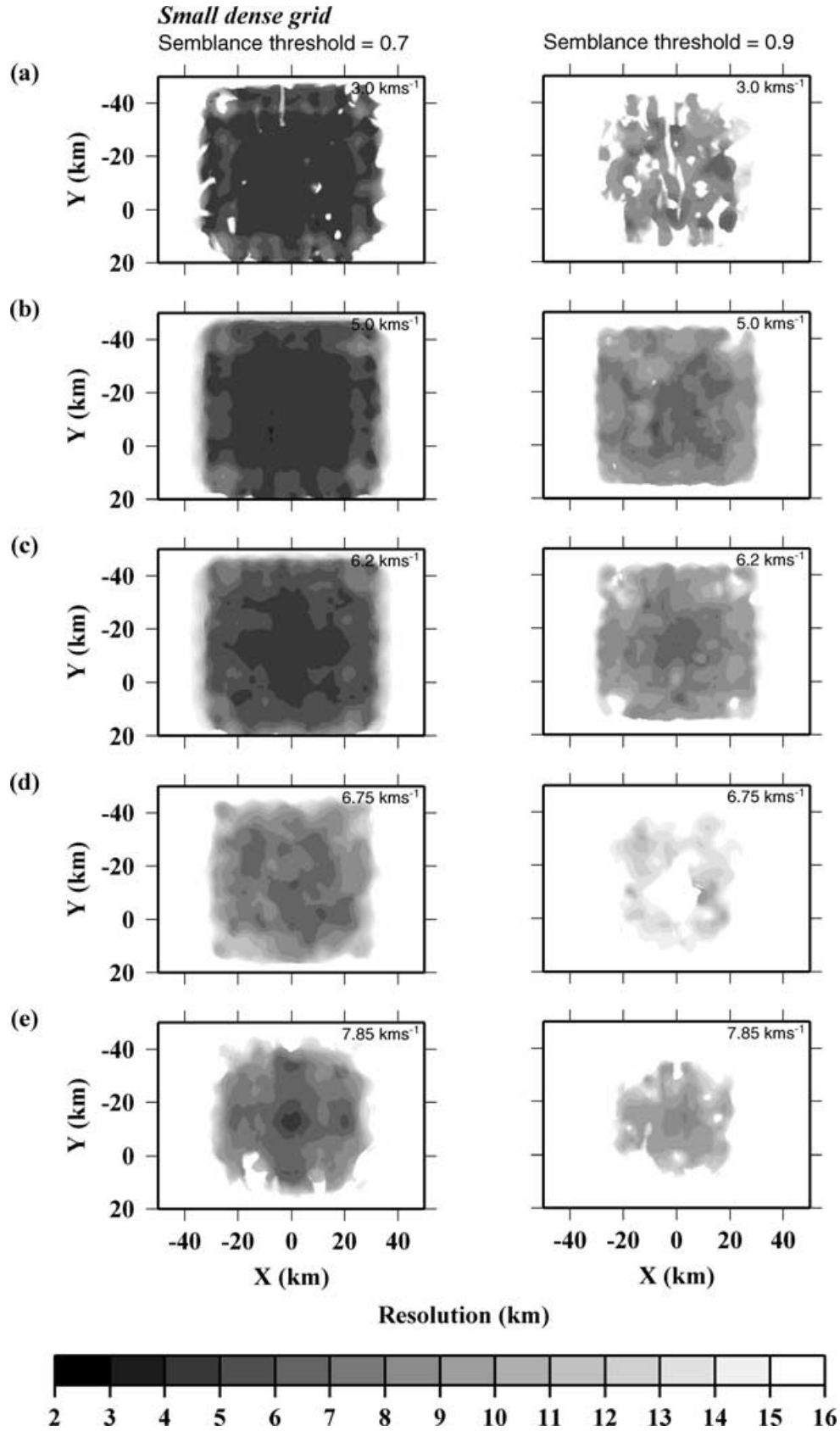

Figure 7. *Small dense grid* geometry. As for Fig. 4. Note the improved resolution at all crustal levels compared with the *Small grid with diagonals* geometry which indicates that profile separation has more importance than instrument separation (*cf*. Fig. 9). Coverage and resolution, in both velocity and magnitude, are generally more even over a larger area and to deeper structural levels. The results of this geometry test highlight the effect of seabed geometry on data coverage and resolution, particularly so for the 0.9 semblance plots (magnitude) down to mid-crustal levels.

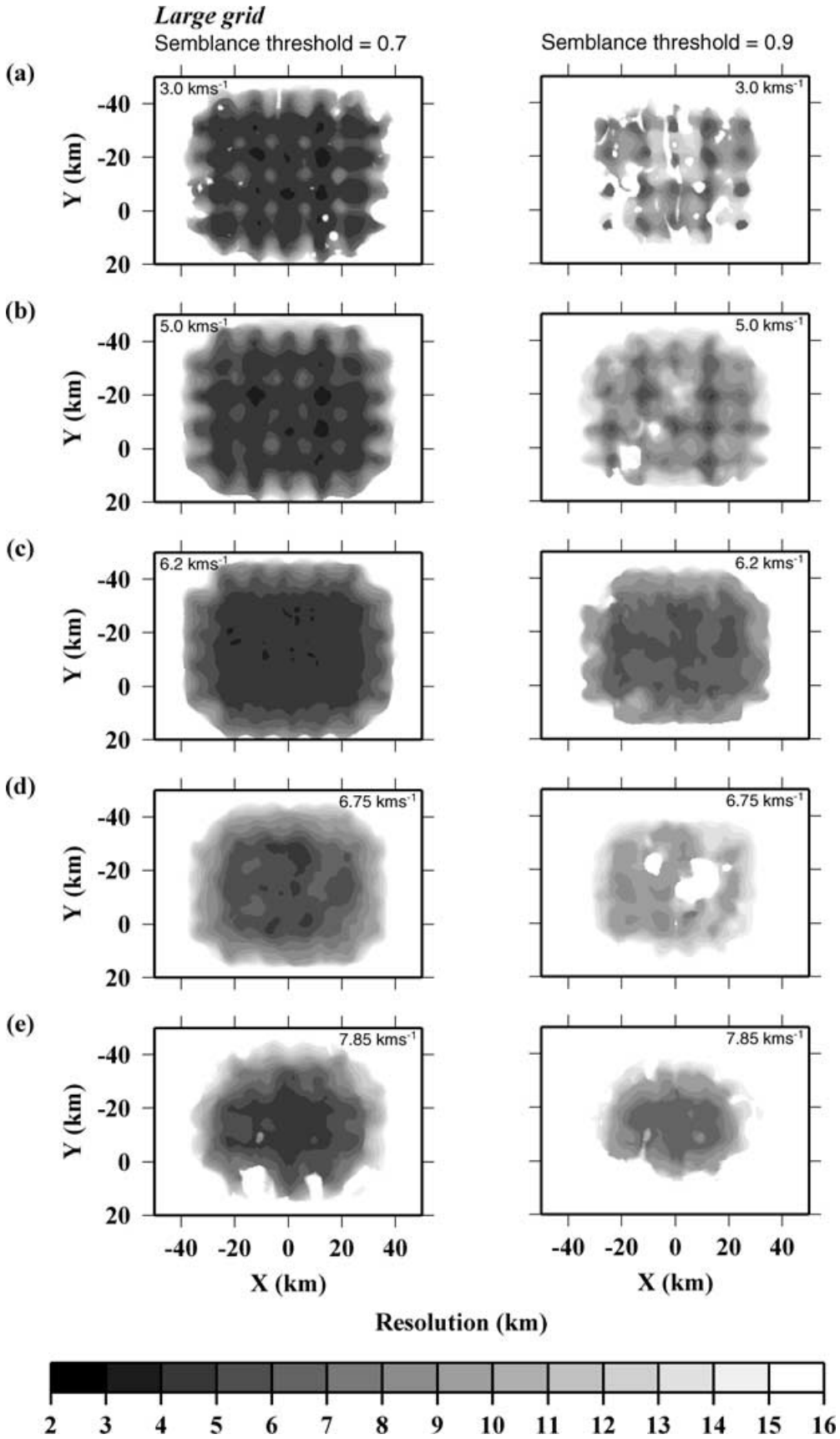

Figure 8. *Large grid* geometry. As for Fig. 4. Note that the correlation between resolution and shot profile and instrument location is much less pronounced than for the *Small grid* geometry but still exists at shallow levels. Resolution is better than 5 km over the principal target and throughout the lower part of the crust and into the upper mantle.

controlled largely by the lateral extent and depth of the primary target of a particular experiment and a grid spacing that will provide adequate resolution coverage at shallow depths.

In this context, we will return to the issue of shot and receiver domain sampling. The *Large sparse grid* geometry (Fig. 3f) may be used to investigate the effect of increasing the sampling interval in the shot domain, i.e. reducing the number of shot profiles to that of the *Small grid*-type geometries. Comparison of Fig. 9 with Figs 5, 6 and 7 suggests that the *Large sparse grid* geometry provides slightly better resolution than the *Small grid* geometry, no better resolution than the *Small grid with diagonals* geometry and worse resolution than the *Small dense grid* geometry, particularly so in the shallower crust. These results imply that, in this case and in resource terms, it is a far better use of resources to increase the number of shot profiles than it is to increase the number of instruments.

Coupled with the increase in instrument numbers over recent years, survey objectives are beginning to focus on much finer-scale detail than was previously achievable, e.g. absolute porosity and its alignment, or the correlation of seismic structure with the geological framework provided by well logging, both as a potential means of investigating tectonic processes and crustal evolution. To this end, considerably more instruments are being deployed over a limited area and the separation between adjacent shot profiles is becoming much reduced. The purpose of the *Dense grid* geometry (Fig. 3g) is to simulate such acquisition. As the resolution plot (Fig. 10) clearly shows this geometry, unsurprisingly, is far superior to all of the others considered thus far. Resolution is better than 3–4 km throughout most of the crust (Figs 10a–c) and in the uppermost mantle (Fig. 10e) within the entirety of the area surveyed. Likewise, the resolution of anomaly magnitude (Fig. 10 right) is similarly improved and both show no instrument or profile location bias at any structural level. However, this effectively ideal coverage comes at the price of a significant increase in the cost of acquisition, in terms of not only the number of instruments required but also the number of shot profiles, and also computational resources associated with data analysis. This point will be discussed further in Section 4.

3.3 Other patterns

The correlation between regions of high resolution and instrument position at shallow levels for the grid geometries described above is, in part, a function of the restricted range of ray azimuths in the uppermost crust arising from the regular geometry of instrument deployment positions and the shooting of profiles which traverse these instruments in a 2-D sense. The *Star* geometry (Fig. 3h) is investigated as a possible means of removing this 2-D 'bias', and as a means of providing greatly improved azimuthal coverage in the uppermost crust as would be required to investigate fracture or porosity extent or preferential alignment. The resolution for this geometry is shown in Fig. 11. Although there is a degree of variability of resolution at shallowest levels which correlates with instrument and shot positions, this effect is far less pronounced than any of the grid geometries despite a comparable instrument spacing. Resolution in the lower crust and uppermost mantle is similar to that for the *Small grid* geometry shown in Fig. 5, although the region of good resolution is much more restricted in area, despite requiring only two extra instruments and the fewest shots of all the geometries considered. However, given the generally superior resolution at shallower depths, this star-shaped geometry would be preferable to a grid when instrument numbers and ship time are limited, or for targets which extend vertically throughout the crust but are of a limited lateral extent, or are known to express anisotropic characteristics. The advantages of the *Star* geometry are generally only applicable to targets of lateral dimensions similar to, or smaller than, the internal 'footprint' of this instrument pattern. If a target exceeds this then multiple, overlapping deployments of the same geometry may provide a cost-effective solution.

To demonstrate the concept of overlap, the resolution of two deployments of the *Star* geometry (Figs 3i and 12) was considered, as this geometry is particularly appropriate for a long, thin target such as the example CVFR. Again, by comparing Figs 5, 11 and 12 for the *Small grid*, the *Star* and *Overlapping star* geometries respectively, it can be seen that the resulting coverage is even and better than 4 km for the majority of crustal layers and the corresponding velocity anomaly magnitude resolution is also much improved. This example clearly shows that a dense coverage at good-to-high resolution can be built-up progressively by the repeated deployment of a relatively few instruments and the careful choice of instrument location. The same approach to acquisition may be applied to much wider targets by progressively building-up the coverage by simply acquiring sufficient laterally overlapping regions, and perhaps including profiles at sufficient offset distances (occupied by previous or subsequent instruments and shot profiles to provide near-surface constraint), to ensure deep crust and upper-mantle arrivals. This approach is shown in Fig. 13 (and *cf*. Fig. 3i) by the *Large overlapping stars* geometry whose resolution plot should be compared with those for the *Small dense grid* and *Dense grid* geometries (Figs 7 and 10 respectively).

The final geometry considered is the *Star* geometry in combination with a number of perpendicular and parallel lines of instrument deployments and shot profiles. This *Combined star and grid* geometry and the resulting resolution are shown in Figs 3(j) and 14 respectively. Comparison with the resolution for the *Large grid*-type geometries (Figs 8 and 9), which require the same number of instruments, reveals that the coverage and resolution are better for this geometry, especially as it covers a significantly wider area. In addition, the resolution is much more consistent in layer 2A, layer 2B/C and the top of layer 3, and significantly improved for the lower crust and uppermost mantle levels. The irregular, pseudospiral pattern of shots and instruments also provides good azimuthal coverage at all structural levels, which is desirable for any investigation of crustal anisotropy. For this particular geometry, a number of shot profiles are located at $\sim$20 km offset from some instruments, and have been included to provide deep crustal and upper-mantle arrivals in the region beneath the ridge-axis, with a resulting improvement in both velocity anomaly and velocity anomaly magnitude resolution at these depths. However, it should be noted that the resolution around the edges is less well constrained than elsewhere, although it is not unconstrained by any means. The resulting potential ambiguity in anomaly location must be weighed against the fact that the inversion methods adopted assume that the initial model represents a reasonably good estimate of the gross structure. If the shallow structure in these regions has some alternative constraint for initial model creation then it can be assumed that that the ambiguity in these regions will be manifest as slightly overestimated resolution at depth simply because the shallow crustal structure is more uncertain at the model edges. However, the target structure lies well within the region defined by the instruments and this region is well resolved. Therefore, provided that the ambiguity (or error) at the edges of the model is taken into account as part of the interpretation process, the results/models provided by such a geometry should be valid and reliable, provided that it is tailored to the shape and depth of the target.

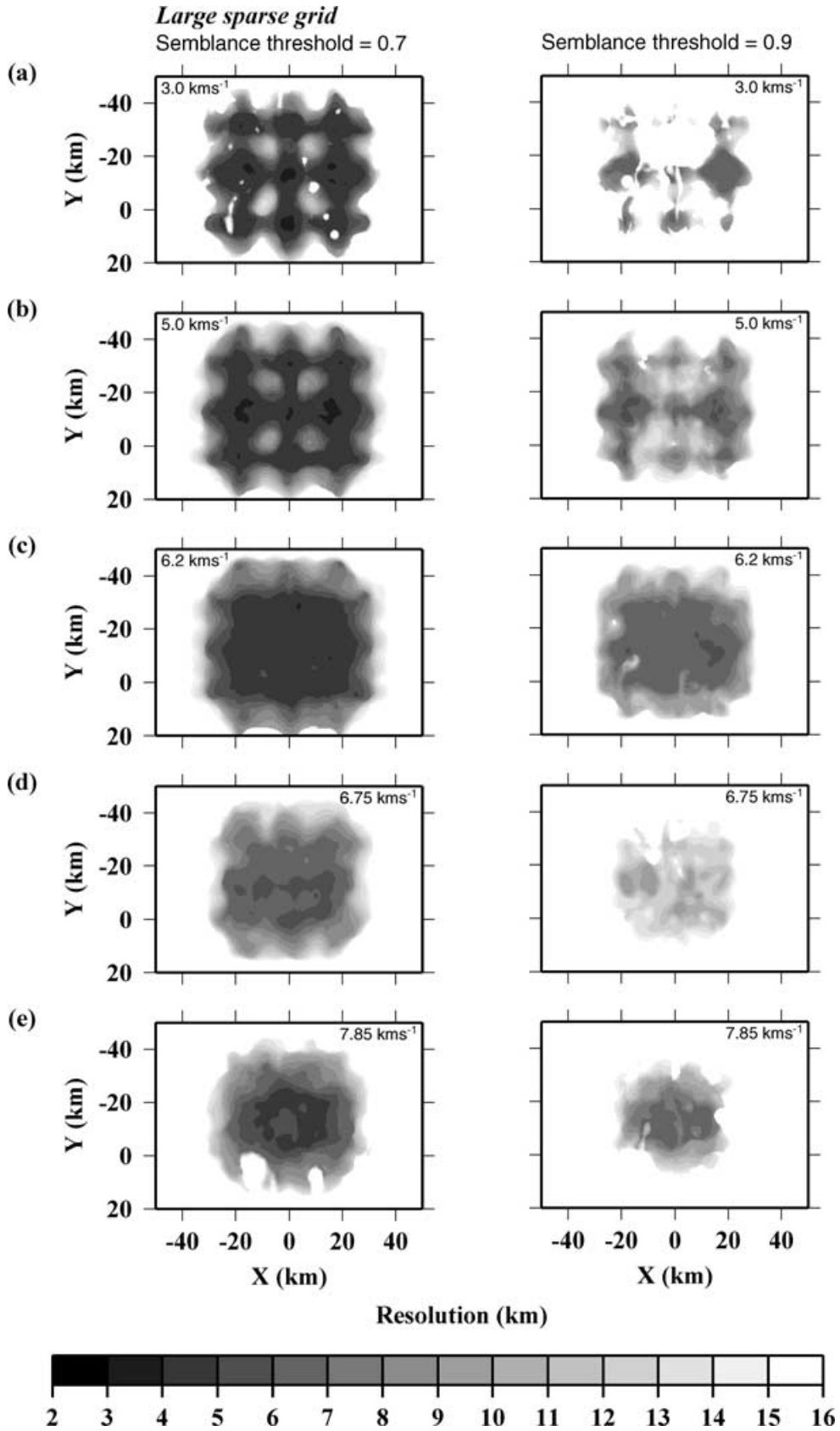

Figure 9. *Large sparse grid* geometry. As for Fig. 4. Note that the correlation between resolution and shot profile and instrument location is much less pronounced than for the *Small grid* geometry but still exists at shallow levels, by contrast to the *Small dense grid* geometry which produces a better result. Resolution is better than 5 km over the principal target and throughout the lower part of the crust and into the upper mantle.

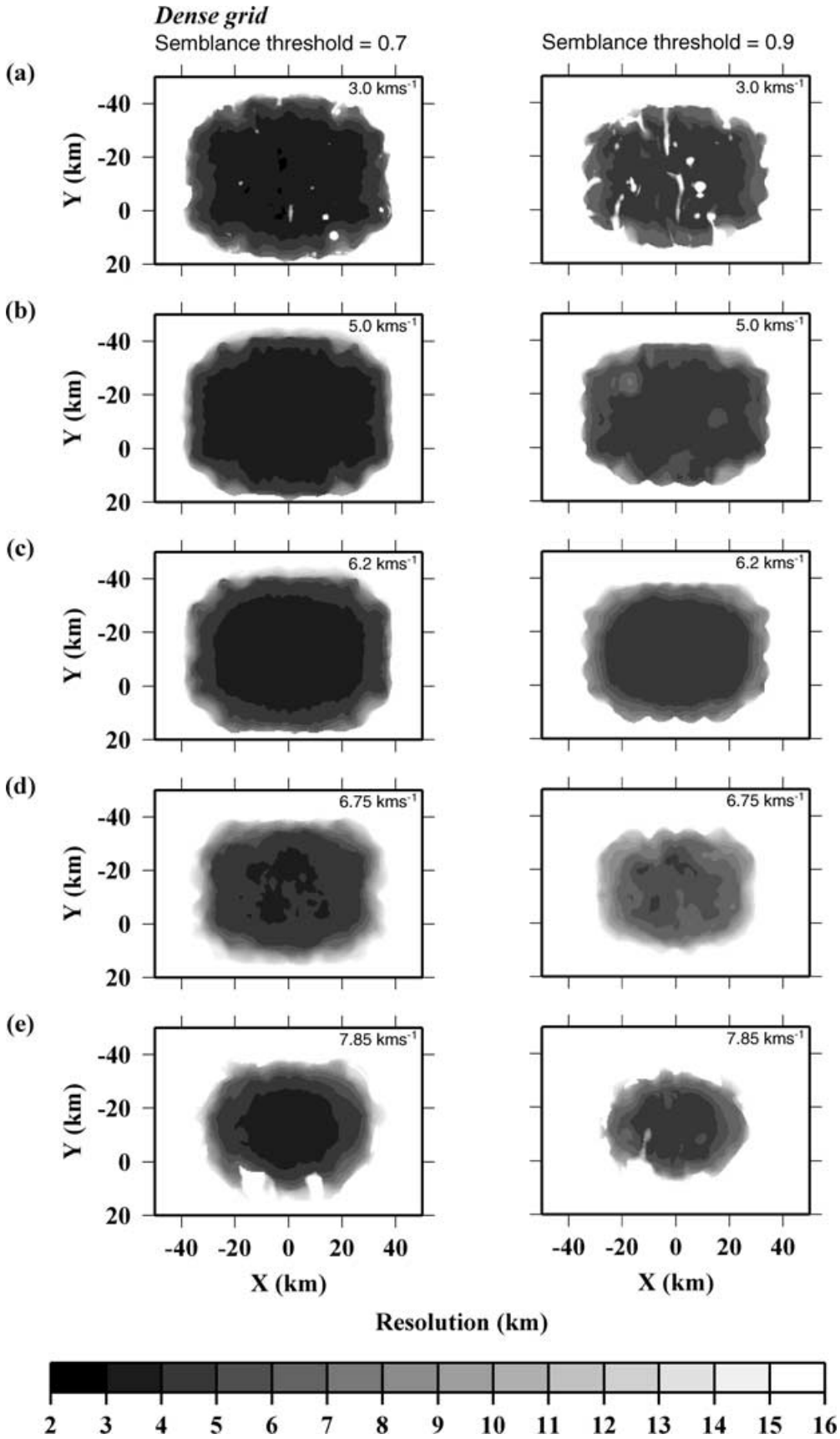

Figure 10. *Dense grid* geometry. As for Fig. 4. Note that this geometry results in good resolution and even coverage at all crustal and uppermost mantle levels throughout the entire survey area. Of note also, at shallow levels, is the effect of the irregular seabed topography on the resulting coverage.

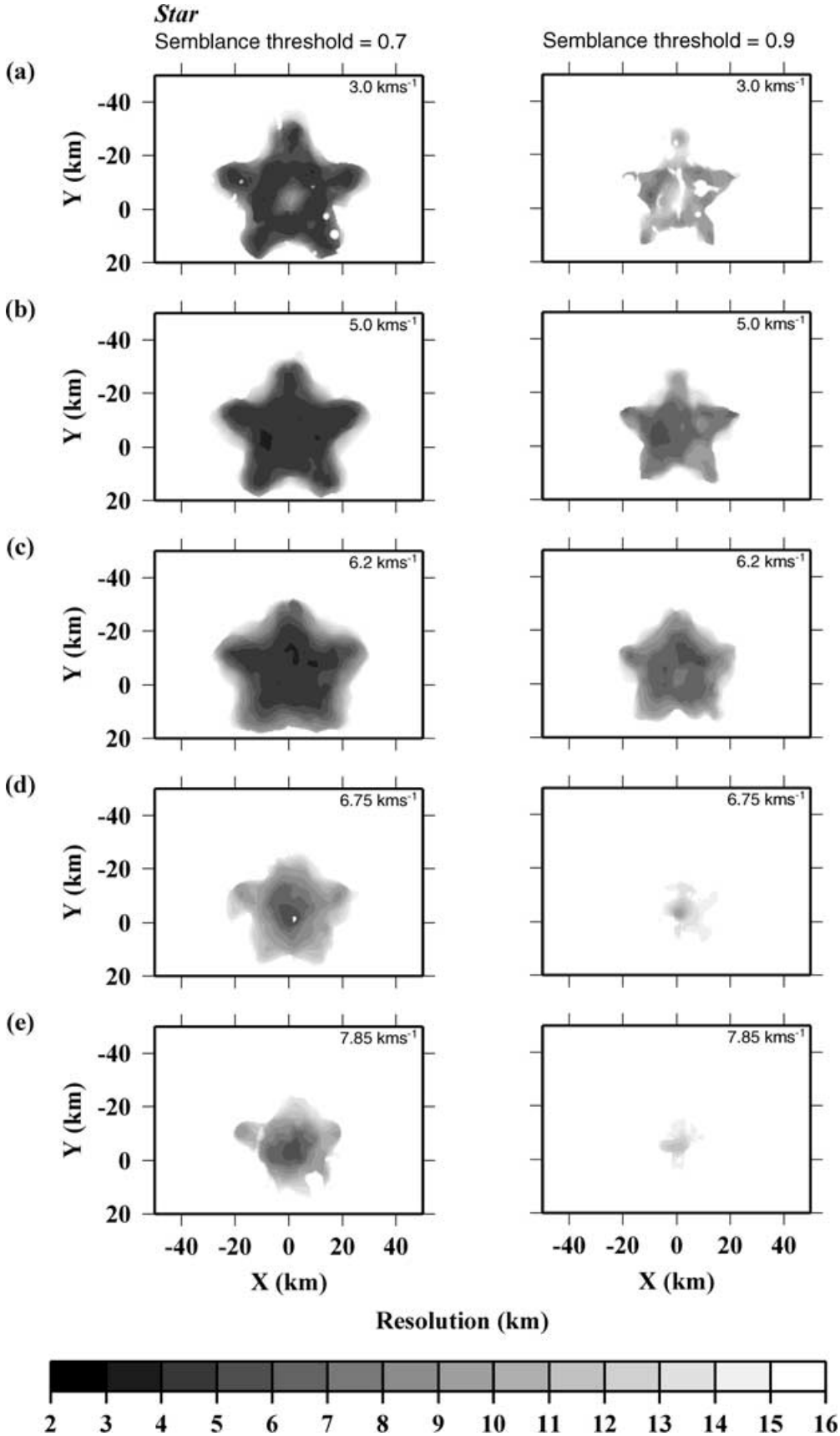

Figure 11. *Star* geometry. As for Fig. 4. Note that this geometry results in good resolution and even coverage at all shallow levels, although over a generally limited area. The resolution is better than 4 km down to mid-crustal levels and better than 8 km down into the uppermost mantle.

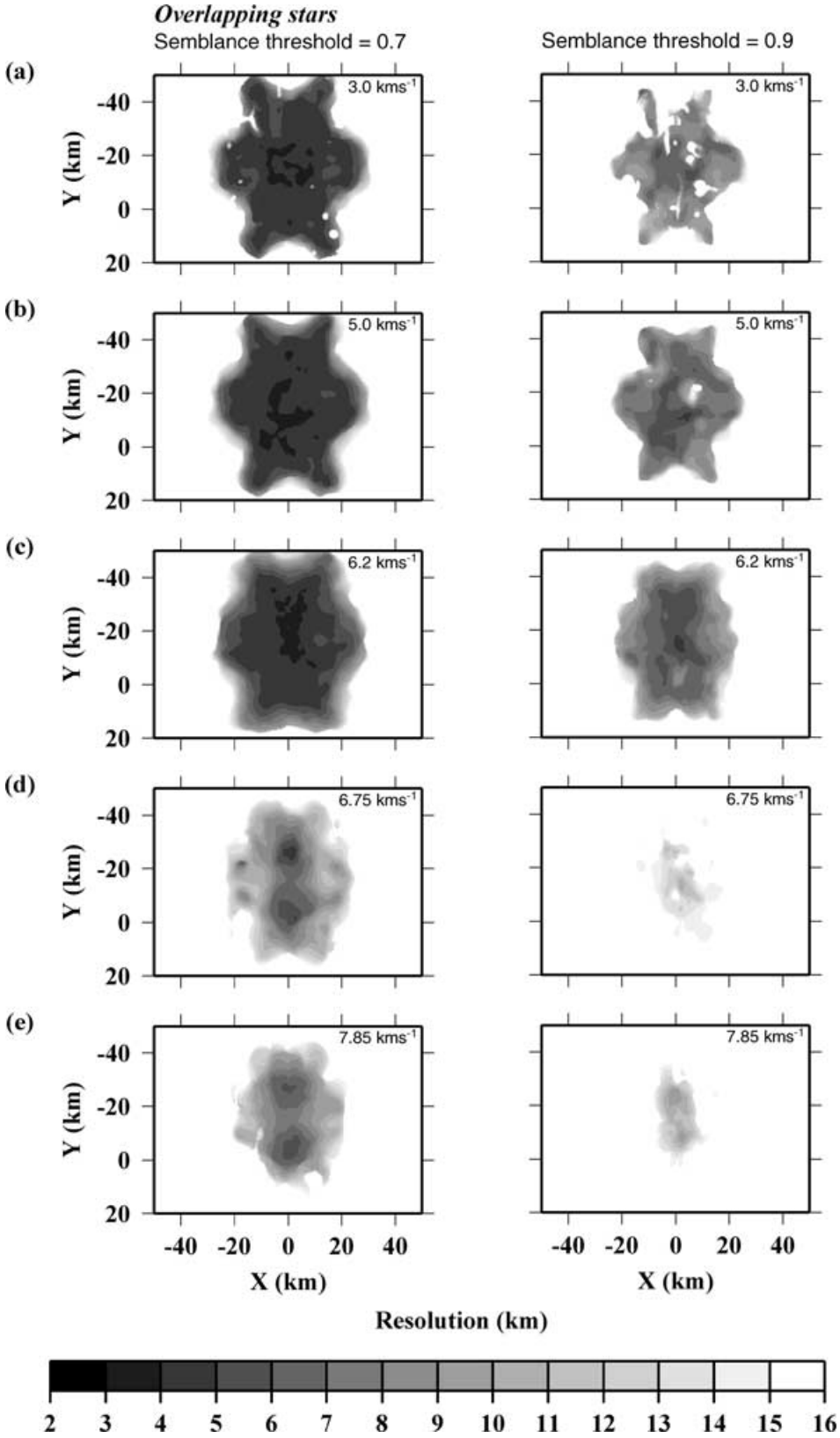

Figure 12. *Overlapping stars* geometry. As for Fig. 4. Note that good coverage may be achieved by progressively combining that achieved through a number of overlapping deployments of a simple geometry such as the *Star* geometry shown in Figs 3(h) and 11, with 2-D profiles shot between pairs (or more) of instruments. By deploying the simple *Star* geometry four times the equivalent coverage and resolution of the *Dense grid* (Figs 3g and 10) may be achieved for the majority of crustal levels. Better coverage and resolution at deeper levels may simply be achieved by shooting a number of profiles at the lateral extremes of the survey area into each *Star* geometry deployment, or by deploying an additional areally enlarged *Star* geometry (plus additional shot profiles) that covers the entire survey area. See Fig. 13.

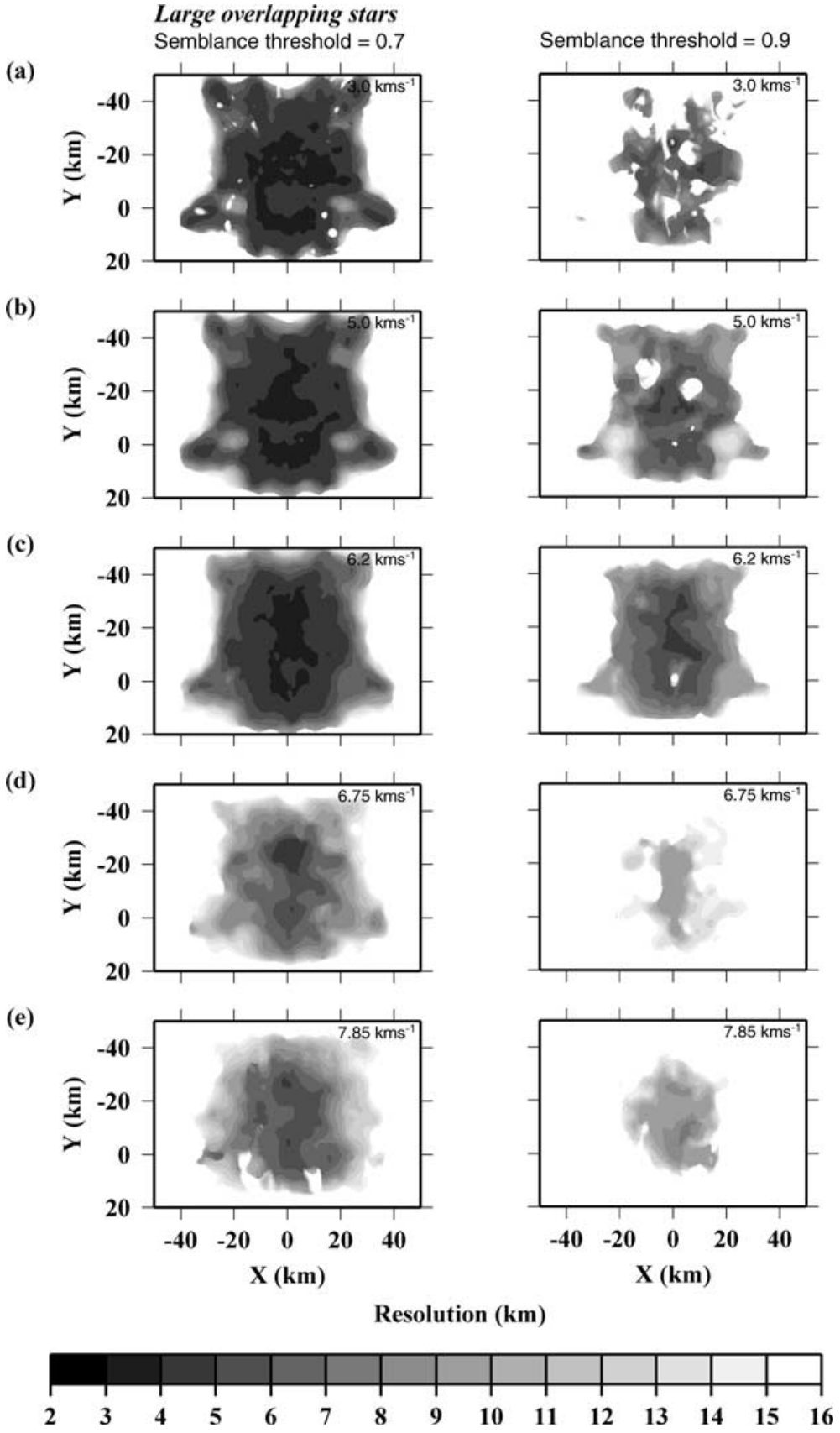

Figure 13. *Large overlapping stars* geometry. As for Fig. 4. Note that in this case coverage is built up progressively by the overlap of three *Star* geometries, one of which is areally sufficiently large to encompass the remaining two (*cf*. Fig. 3i). Resolution equivalent to the *Overlapping stars* geometry is achieved at all crustal levels, but over a larger 'footprint' area as would be expected.

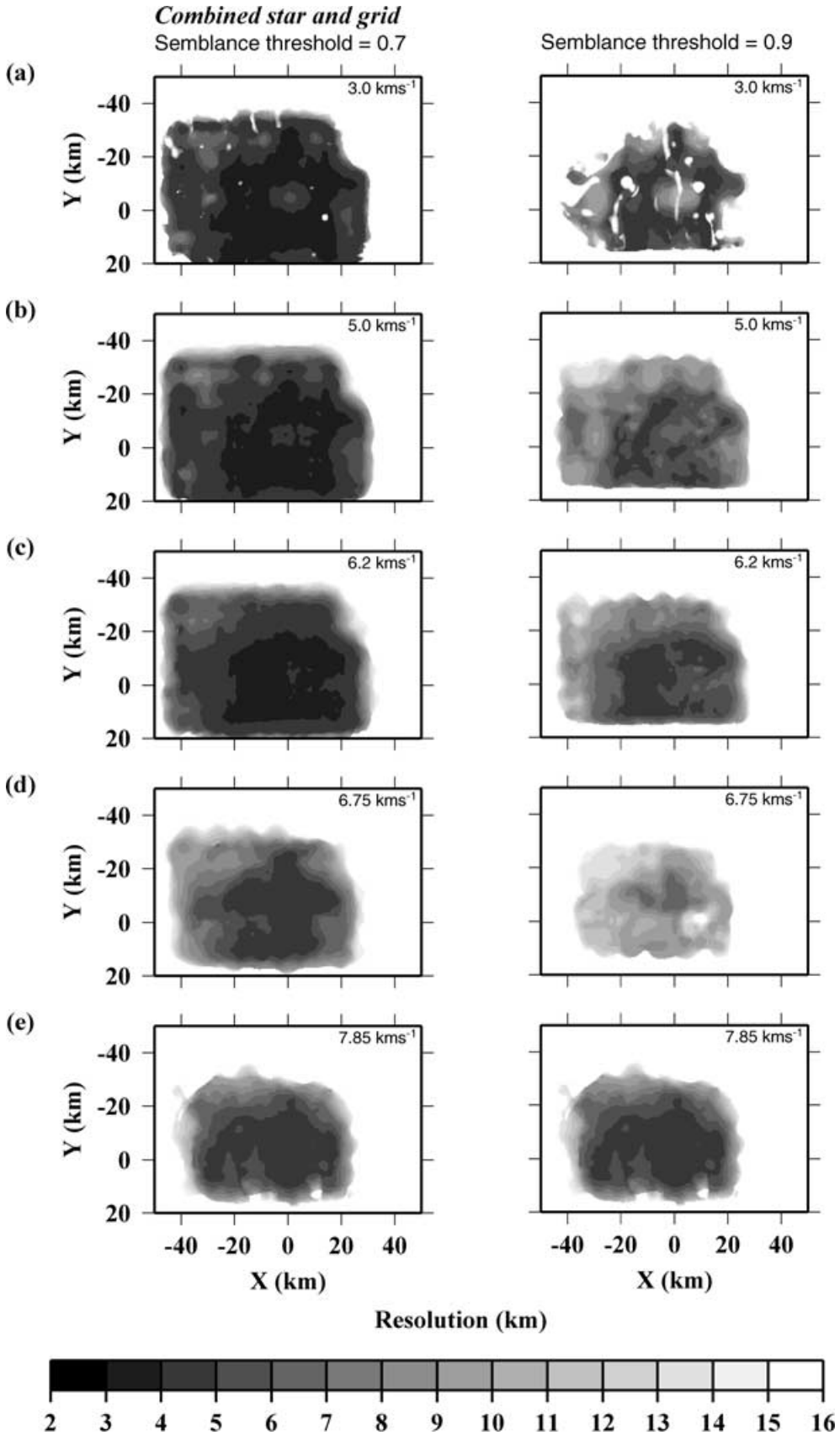

Figure 14. *Combined star and grid* geometry. As for Fig. 4. Note that resolution is better than 3 km at shallowest levels and more even throughout the entire survey area. A resolution of better than 4 km persists throughout the crust and into the uppermost mantle. This geometry also provides good resolution and coverage over a wider area than the *Dense grid*.

4 DISCUSSION

Although the geometries discussed in the above section are merely examples of the broad range of other possibilities that are available, and obviously some are more suitable or sensible than others, comparison of the resolution plots does suggest that such approaches should at least be considered when resources are limited. Comparison of the resolution tests for the eleven example experimental geometries have shown that a number of factors need to be considered when choosing or designing an appropriate geometry for any particular experiment. These features may be summarized as a series of questions as outlined below:

1. *What are the lateral dimensions of the target and its depth below surface*?

Probably the most important criteria to determine before an acquisition geometry is selected or designed are the characteristic features of the target and, most importantly, its depth, or range of depths, below the surface. If the primary target is located at a certain depth below the surface it is essential that adequate and even sampling of the region shallower than the target is obtained such that an accurate representation of it may be made in the initial model, and so that deeper anomalies recovered during the inversion process are not upwardly or laterally smeared. In addition, it is also necessary to ensure that the region beneath the target is adequately sampled to ensure that anomalies recovered at depth do not merely reflect uneven data coverage.

The controlling factors on shallow data coverage are the instrument and shot profile spacing and the water depth; the latter determining not only the shot-receiver offset at which intra-crustal arrivals become emergent from the direct water wave but also possible regions of low, or no, data coverage. The instrument spacing and shot profile location should thus be chosen to provide even coverage at shallow levels and also include 2-D profiles, analysis of which provides information for creation of the initial model. To provide even sub-target coverage instruments need to be located sufficiently distant laterally from the target. Shots should also be fired not only from the opposite sides of the target but also opposite sides adjacent to each instrument to provide shallow control on sub-instrument structure.

2. *What are the physical features of the target*?

It is important to consider the physical features and characteristics of the target itself and whether these features have a preferential alignment, or orientation, before the geometry is finally decided, e.g. the nature of absolute porosity or alignment of fracture patterns. In turn, it is also important to consider the possibility of anisotropic variation in velocity structure when constructing initial models and interpreting resolved anomalies. Thus, the experimental geometry should be designed such that any azimuthal variation due to the target, and/or linear bias due to the shooting of shots along linear profiles into instruments deployed primarily along linear trends, may be resolved. Apart from aligning shot profile and/or instrument locations oblique to likely preferential orientation directions, an additional approach might be to deploy a number of multi-component instruments (rather than single, e.g. hydrophone only) throughout the survey area, capable of recording *S*-waves and *P–S* mode converted arrivals which enable particle motion studies.

3. *What is the water depth and seabed topography*?

An important consideration when designing an experimental geometry is the nature of the seabed topography and, in particular, the effect this will have on the data coverage, i.e. will the topography of the seabed create patchy, or uneven, shallow coverage? Such uneven coverage may result in holes in the recovered anomaly pattern (see Figs 7 , 8, 10 and 14) or a higher uncertainty in these regions of the resulting model. Thus, if a regular grid-like instrument deployment and shot profile pattern is adopted it may be necessary to modify it to accommodate the nature of the seabed topography. A further issue in this context is the water depth, the associated arrival time of the direct water wave with respect to the emergence of shallow crustal arrivals, and the ability to pick the travel times of these phases at near offset, as this will affect subsequent resolution immediately adjacent to each instrument.

4. *What will be the effect on coverage of instrument failure or loss*?

When designing any acquisition configuration, no matter how densely populated with instruments and shot profiles, it is essential to factor in the consequences of single or multiple instrument loss or failure to record data, and design the geometry with a degree of redundancy in critical areas.

5. *What information is required for initial model construction*?

To create an initial model for inversion it is necessary to have an indication of the vertical variation in velocity structure, preferably so throughout the survey area, such that the inversion process largely resolves lateral velocity variation. The simplest approach to determining the vertical variation, normally related to intra-crustal layering, is to incorporate within the geometry at least one, and ideally more than one, 2-D profile which may be forward ray trace modelled. If the target has any structural trend these 2-D profiles should be located perpendicular to strike and, ideally, connected by an along-strike profile to assess along-strike variability to determine whether or not a 1-D initial model is adequate or whether a degree of two-dimensionality also needs to be incorporated (see Day *et al.* 2001).

6. *How may inversion artefacts be identified and minimized*?

Inversion artefacts are normally related to the upward and lateral smearing of recovered anomalies resulting mainly from an irregular density of data coverage. However, they can also arise from inversion bias resulting from a large percentage of inline shots and instruments (Day 2001). Thus, to minimize the potential of artefacts being generated it is preferable to adopt an acquisition geometry that provides even shallower-than-target coverage but does not contain a high percentage of instruments located along individual shot profiles. In other words, serious consideration should be paid to the creation of a geometry that has a large degree of asymmetry in both instrument deployment and shot profile location.

7. *How many shots and instruments are necessary, or desirable, to achieve the required resolution*?

In an ideal world it would be desirable to deploy a geometry along the lines of the *Dense grid* for many geological targets. However, as previously stated, it is not necessarily possible to have access to such a level of resource for a variety of reasons that normally ultimately relate to the level of available funding. The primary purpose of this paper is to show that smaller-scale approaches to acquisition can provide invertible data sets and, consequently, meaningful and interpretable models of an appropriate resolution to characterize a particular target.

To demonstrate this point the eleven experimental geometries have been costed in a generalized manner in terms of required ship days, to make the comparison independent of the actual cost of a nation-specific ship day. The costs of multiple deployments have been included where appropriate. Instrument costs (consumables and staff time) are considered in increasing percentages of a ship day, where the percentages should be viewed in terms of

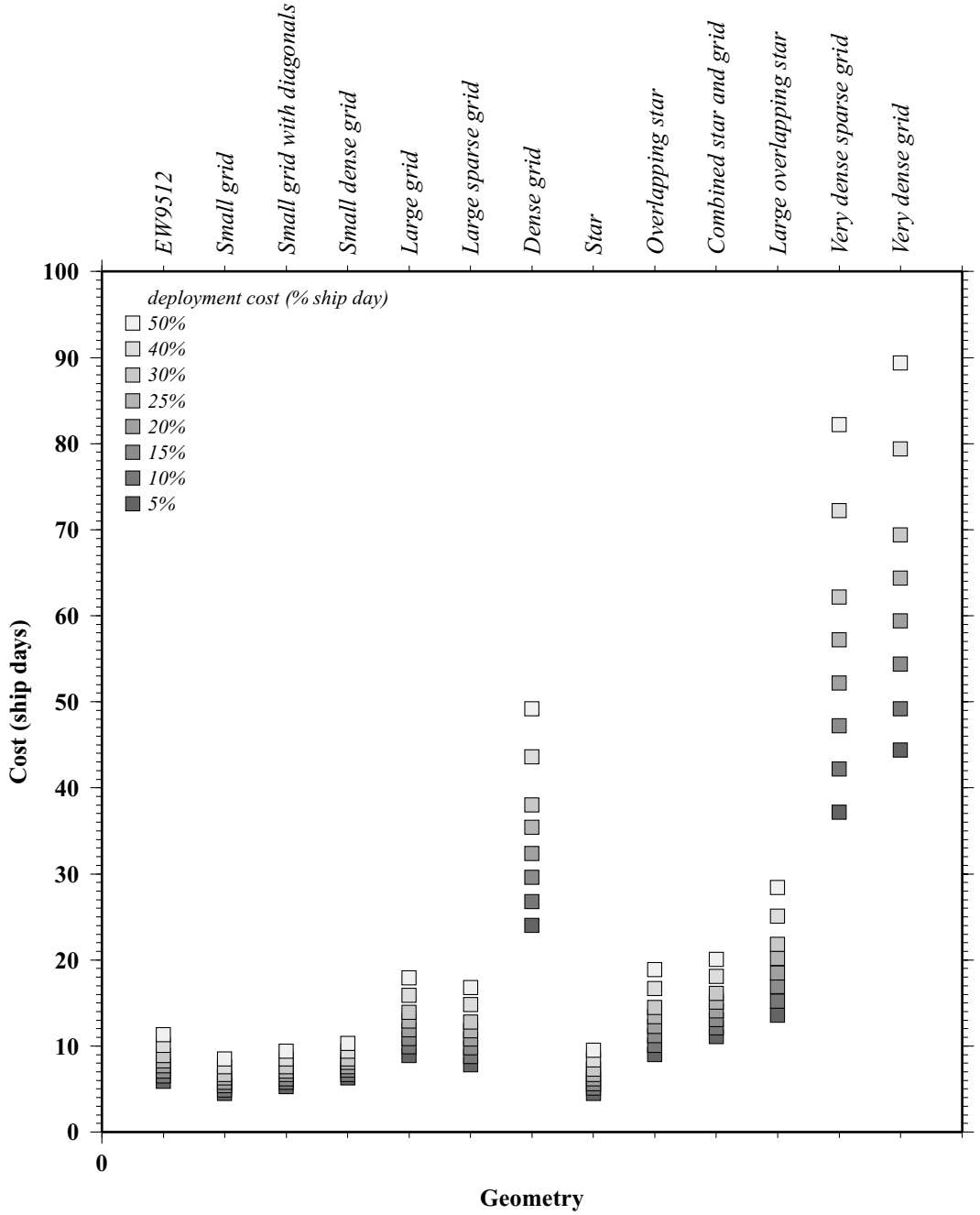

Figure 15. Comparison of relative resource usage for each example experimental geometry. Total cost, expressed in ship days, includes shot firing, instrument deployment and recovery and transits between instrument locations. Instrument deployment costs (e.g. batteries, bottom weights etc.) have been calculated at varying percentages of a ship day, which reflects the relative variation in cost between hiring (>30 per cent), inclusion of otherwise unsupported staff time (15–30 per cent depending on number and type of staff) or consumable items only (<15 per cent depending on instrument type). See Table 2 for details.

representing solely consumable costs (<15 per cent bracket), consumable costs and staff time (20–30 per cent) and hiring which includes a profit margin (>30 per cent). The percentages in each bracket reflect the fact that consumable costs are instrument-type specific, and that staff costs are covered in various ways—e.g. as non-grant dependent posts, grant-dependent posts or combinations thereof. Table 2 summaries the results of this costing and Fig. 15 demonstrates the results graphically. Notable geometries to compare are: the *Small dense grid*, the *Large grid*, the *Dense grid*, *Large overlapping stars* and the *Combination star and grid*. The right-hand columns in Table 2 indicate the approximate relative total cost for deployment costs of the order of 10 per cent and 50 per cent of a ship day, while values for other additional percentage costs are shown in Fig. 15. Thus this figure should be considered in relation to Figs 4–14, in order to assess which experimental geometry produces the most even and areally extensive, high resolution coverage whilst providing the best value for money, and in addition to the percentage deployment costs of the particular instruments available. To put the example geometries discussed in this paper in relative cost context with those for considerably denser grids using 100 instruments, two further geometries have also been costed in Table 2 and graphically shown in Fig. 15 for comparison. The *Very dense sparse grid* has

Table 2. Summary of nominal time and resource implications required by each synthetic experimental geometry in ship days. The 'cost' of an instrument deployment is included as a percentage of a ship day, where increasing percentages reflect the inclusion of staff costs and accessing instruments by hire agreements. Shot spacing is 200 m and shooting speed 9 km h^{-1}.

Geometry	Number of instruments	Number of deployments	Average instrument spacing (km)	Approximate total number of shots	Approximate total profile length (km)	Approximate total time to shoot (hr)	Approximate total time to deploy, recover and transit between instruments (hr)	Approximate total time for acquisition (hr)	Relative cost—instrument deployment @ 10 per cent (ship days)	Relative cost—instrument deployment @ 50 per cent (ship days)
*EW9512**	6	2	10	2500	500	56	72	5.3	6.5	11.3
Small grid	9	1	18	1920	384	43	54	4.0	4.9	8.5
Small grid with diagonals	9	1	18	2820	564	63	54	4.9	5.8	9.4
Small dense grid	9	1	18	3840	768	85	54	5.8	6.7	10.3
Large grid	20	1	12	3100	620	69	120	7.9	9.9	17.9
Large sparse grid	20	1	12	1920	384	43	120	6.8	8.8	16.8
Dense grid	56	1	8	7750	1550	172	336	21.2	26.8	49.2
Star	11	1	15	1300	260	29	66	4.0	5.1	9.5
*Overlapping star**	11	2	15	2600	520	58	132	7.9	10.1	18.9
Combined star and grid	20	1	10	5500	1100	122	120	10.1	12.1	20.1
Large overlapping star	11	3	15	3975	795	88	198	11.9	15.2	28.4
Very dense sparse grid	100	1	4	7750	1550	172	600	32.2	42.2	82.2
Very dense grid	100	1	4	15500	3100	344	600	39.4	49.4	89.4

See text for details and compare with Fig. 14.
*All deployments included in relative costing.

the same number of shots as the *Dense grid* with shot profiles running effectively through alternate instrument positions in both *x* and *y* directions, while the *Very dense grid* has double this number of shots, with profiles running through every instrument position.

For a target of the dimensions of the CVFR, the *Small dense grid* is probably the most cost effective if shallow resolution is required extending into older crust off-axis and down to the uppermost mantle. In addition, if the shallow layers contain characteristic features that result in, or may be investigated by, an anisotropic velocity structure then the *Combined star and grid* geometry with its asymmetric design might also be an appropriate geometry to adopt. However, if instrument numbers are limited then the multiple deployment strategy may prove optimum as shown by the *Large overlapping stars* geometry. This result is highlighted for the CVFR example where the same crustal coverage and resolution as provided by the *Dense grid* may be achieved by four overlapping *Star* geometries resulting in a net saving of ∼20 per cent of the acquisition cost. Comparison of the *Small dense grid* with the *Large sparse grid* also indicates that if resources are limited (and there is a means by which to constrain shallow structure) it is better to shoot additional profiles rather than deploy additional instruments.

5 SUMMARY

Although this analysis has concentrated on 3-D data acquisition at mid-ocean ridges, using the CVFR as an example, the general conclusions and considerations apply to most scenarios. In particular it is desirable to design experiments which allow adequate resolution at all structural levels down to the primary target depth as inadequate recovery of velocity heterogeneities at shallower levels has been shown to influence the anomalies recovered at the target depth. Shot and receiver spacing and geometry should thus be chosen such that they provide even and good resolution coverage, particularly so at levels shallower than the target depth. In this context geometry 'footprint' should be considered in relation to target dimensions such that, if resources are limited, shooting additional profiles will most likely result in better resolution than deploying additional instruments. Alternatively, multiple deployments of a smaller geometry to progressively build-up coverage may prove most cost-effective in certain situations. In addition, to avoid 2-D bias in recovered anomalies it is also advisable to incorporate a degree of asymmetry in shot profile location and instrument deployment position and to provide a high degree of azimuthal coverage, again at all levels. When selecting the most appropriate geometry the cost implications, in terms of the requirements each entail for ship time and instrument numbers, should always be considered with respect to making the best use of available resources.

ACKNOWLEDGMENTS

Figures were created using the Generic Mapping Tool of Wessel & Smith (1995). We thank Colin Zelt for the use of his tomography code. AJD was financially supported via a Natural Environment Research Council studentship (GT4/97/71/ES). The helpful comments of two anonymous reviewers greatly assisted in improving the clarity of this paper.

REFERENCES

Collier, J.S. & Sinha, M.C., 1992. Seismic mapping of a magma chamber beneath the Valu Fa Ridge, Lau Basin, *J. geophys. Res.,* **97,** 14 031–14 053.

Day, A.J., 1997. Seismic reflection imaging and modelling of the melt lens beneath the Valu Fa Ridge, *unpublished M.Sc. thesis,* University of Durham, UK.

Day, A.J., 2001. Seismic imaging of crustal structure at mid-ocean ridges: a three-dimensional approach, *unpublished PhD thesis,* University of Durham, UK.

Day, A.J., Peirce, C. & Sinha, M.C., 2001. Three-dimensional crustal structure and magma chamber geometry at the intermediate-spreading, back-arc Valu Fa Ridge, Lau Basin—results of a wide-angle seismic tomographic inversion, *Geophys. J. Int.,* **146,** 31–52.

Peirce, C., Sinha, M.C. & Constable, S., 1996. Controlled source electromagnetic and seismic investigation of the Valu Fa Ridge, Lau Basin, SW Pacific, *R/V Maurice Ewing* 9512 Cruise Report, unpublished, University of Durham, p. 56.

Sohn, R.A., Webb, S.C., Hildebrand, J.A. & Cornvelle, B.D., 1997. Three-dimensional tomographic velocity structure of upper crust, Co-Axial segment, Juan de Fuca Ridge: Implications for on-axis evolution and hydrothermal circulation, *J. geophys. Res.,* **102,** 17 679–17 695.

Toomey, D.R., Solomon, S.C. & Purdy, G.M., 1994. Tomographic imaging of the shallow crustal structure of the East Pacific Rise at 9° 30′ N, *J. geophys. Res.,* **99,** 24 135–24 157.

Turner, I.M., 1998. Crustal accretionary processes at mid-ocean ridges—Valu Fa Ridge, Lau Basin, *unpublished PhD thesis,* University of Durham.

Turner, I.M., Peirce, C. & Sinha, M.C., 1999. Seismic imaging of the axial region of the Valu Fa Ridge, Lau Basin—the accretionary processes of an intermediate back-arc spreading ridge, *Geophys. J. Int.,* **138,** 495–519.

Vidale, J.E., 1990. Finite-difference calculation of travel times in three dimensions, *Geophysics,* **55,** 521–526.

Wessel, P. & Smith, W.H.F., 1995. New version of the Generic Mapping Tools released, *EOS Trans. Am. geophys. Un.,* **76,** 329.

Zellmer, K.E., Taylor, B., Martinez, F. & Goodliffe, A., 1998. Complexities in the seafloor spreading history of the Lau Basin, *EOS Trans. Am. geophys. Un.,* **79,** No. 45, 908.

Zelt, C.A., 1998. Lateral velocity resolution from three-dimensional seismic refraction data, *Geophys. J. Int.,* **135,** 1101–1112.

Zelt, C.A. & Barton, P.J., 1998. Three-dimensional seismic refraction tomography: A comparison of two methods applied to data from the Faeroe Basin, *J. geophys. Res.,* **103,** 7187–7210.